Journal of Sound and Vibration 511 (2021) 116342

Contents lists available at ScienceDirect

Journal of Sound and Vibration

journal homepage: www.elsevier.com/locate/jsvi

Time-domain numerical continuation of periodic orbits for harmonically forced hysteretic nonlinear systems with Iwan joints

Seyed Iman Zare Estakhraji *, Matthew S. Allen

University of Wisconsin, Madison, United States of America

ARTICLE INFO

Keywords:
Iwan model
Hysteresis
Coulomb sliders
Continuation method
Frictional devices
Steady-state response

ABSTRACT

Coulomb sliders are used widely in order to model frictional interfaces. In many applications, the nonlinear Frequency Response Functions (FRFs) of these systems is desired, but it is extremely computationally expensive to use time-domain integration methods to compute the steady-state response. The nonlinear force and stiffness of these devices depends on the position of sliders, and the implicit nature of the slider positions makes these systems hysteretic and therefore non-trivial to address using conventional continuation methods. This paper proposes a novel numerical method, dubbed "Hysteresis Identification via Reversal Points or (HIRP)" that can compute the steady-state harmonically forced response of frictional nonlinear systems. For this purpose, a quasi-static algorithm is introduced which can evaluate the state of sliders at any time based on the reversal points over a period. This reduces the number of state variables needed in the continuation routine by at least an order of magnitude. The method has been tested by computing the harmonic response of a hysteretic system with multiple Coulomb sliders. The method is evaluated on multi-degree of freedom systems with Iwan joints, demonstrating that the method can be a valuable tool for predicting the nonlinear, steady-state response of hysteretic systems.

1. Introduction

The harmonic forced vibration of nonlinear systems has been of interest for at least sixty years [1–4]. Most engineering structures can experience dry friction, for example in bolted joints [5–8], or between other surfaces such as the interfaces between bladed disks [9–12]. Under oscillatory loads, one can observe a transition between stick and slip, see for example the applications presented in [13,14]. Fig. 1 illustrates the problem using a finite element model of a system consisting of two beams that are joined by bolts at their free ends. When the bolts are tightened, the beams come into contact in a region near the bolts (shown in red). Suppose that the structure then vibrates in its first mode. The figures show that material near the edge of the contact interface begins to slip (shown in green). At first, the normal load applied on the bolts dominates and the slip region is very small, referred to as (micro-slip) [15]. This results in a slight reduction of the stiffness of the joint and the friction forces at the surfaces dissipate energy and introduce hysteresis [16]. As the vibration amplitude increases, the slipping region spreads towards the center of the bolt causing more severe nonlinear behavior. In extreme cases the joint can exhibit macro-slip, where the entire interface is slipping and the contacting surfaces undergo bulk motion relative to one another [17]

Indeed frictional devices such as bolted joints typically provide much of the damping in built up structures and at times have been intentionally employed to damp the resonant response of such systems, although they remain poorly understood and so this has proven challenging. In order to effectively design or optimize structures to achieve noise reduction or vibration control [18,19],

* Corresponding author.
E-mail addresses: zareestakhra@wisc.edu (S.I.Z. Estakhraji), msallen@engr.wisc.edu (M.S. Allen).

https://doi.org/10.1016/j.jsv.2021.116342
Received 8 September 2020; Received in revised form 9 June 2021; Accepted 3 July 2021
Available online 15 July 2021

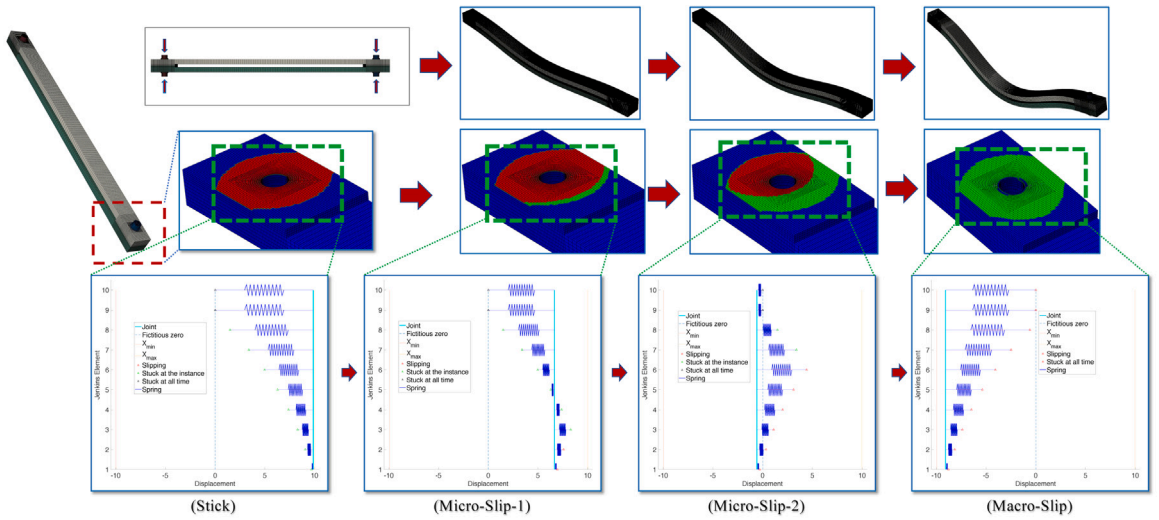

Fig. 1. Schematic representation of stick–slip transition of a nonlinear system with dry friction (bolted joints) over one quarter of a vibration cycle. The areas shown in green are slipping and the areas in red are stuck. As the vibration amplitude increases, the contact regime evolves from stick to micro-slip and then macro-slip. The subplots show the analogous behavior of an Iwan joint. (For interpretation of the references to color in this figure legend, the reader is referred to the web version of this article.)

better computational tools are needed. In this regard, the Frequency Response Function (FRF) is an important quantitative measure of the dynamic behavior with various applications. However, because of the hysteresis phenomena observed in systems with frictional devices, calculation of the FRF of a nonlinear system is not a trivial task. This work proposes an efficient numerical strategy that can compute the steady-state response of frictional hysteretic systems that are subjected to harmonic forces.

In order to model different phenomena such as hysteresis or a stick–slip transition, various friction models have been developed [20,21]. The most common model is the Coulomb friction model, which treats two surfaces as either completely stuck or completely slipping, so the hysteresis loop for the system has a trapezoidal shape. Other models seek to capture additional physics, such as the deformation that occurs before sliding, e.g. the LuGre model [22,23] or the Leuven model [24], and they may also capture the elasticity or other physics that round out the hysteresis loops, as occurs in the Bouc–Wen model [25]. The Coulomb model is implemented in several codes and is used quite frequently in finite element simulations, where it is assumed to hold at a millimeter scale. The parameters for the other models are not derivable from first principles, and so they are not typically applied at the mm-scale; they are used mainly for whole joints or in reduced order models. A recent study found that one needs a very fine mesh near the contact region to use Coulomb friction to model bolted joints [8], so it becomes computationally prohibitive to use this approach for anything but quasi-static or very short duration dynamic simulations.

Gaul et al. [16] used Jenkins elements to simulate a joint by implementing harmonic balance method. Later, Oldfield et al. [26], for the case of two solid blocks held together by a composite bolt–nut component, tried to replicate the hysteresis curved obtained from the finite element model solved in a commercial code by implementation of Jenkins elements. They used a fourth-order Runge–Kutta time integration to calculate the time history response of the Jenkins elements system with one to five sliders. Although they have shown that using Jenkins element can reduce the complexity of the system and replicate the hysteresis behavior, but modeling the more complex systems requires larger number of elements whereas using time integration method for a large number of elements can be excessively expensive.

Iwan made significant contributions in the steady-state response of hysteretic systems [1,27,28] and in 1966 [4], he used a parallel arrangement of Jenkins elements (each of which consists of a Coulomb slider in series with a linear spring) to introduce a new joint model called the Iwan element or Iwan joint. Each Coulomb slider can have a different normal force so that they all slip at a different instants, so a single Iwan joint can model a wide array of phenomena, including the power-law energy dissipation that is often observed in joints [6]. The third row of images in Fig. 1 gives a schematic view of an arrangement of ten Jenkins elements used to represent stick–slip behavior. When only a few of elements are slipping the joint is in micro-slip, and a wide range of micro-slip behavior can be captured by varying the slip force of each Jenkins element. As a result, Iwan elements have been employed extensively by researchers [6,29–33]. They have been shown to provide an ideal elastic/perfectly-plastic hysteresis curve under harmonic force [4,26] and have even been extended to capture random loads [34]. This paper focuses on extending the shooting method to compute the steady-state forced response of hysteretic systems that are modeled with one or more Iwan elements, or with an arbitrary distribution of friction sliders.

The most straightforward way of computing the steady-state response of a hysteretic system would be to use step by step numerical integration to solve the second order differential equation of motion in the time domain. This has been used since late 1980s [35,36]. Responses computed using this approach always include the transient as well as the steady-state response, and because the systems of interest tend to be lightly damped, very long computational times are required for the transient

response to decay so that one can recover the steady-state response. Doing so, relatively small time steps are needed because the contact stiffness values is often relatively high. For non-hysteretic systems, the shooting method [37,38] has been used to predict the periodic solutions and obtain other dynamic characteristics efficiently [39–41]. Then, Peeters et al. [42], proposed an efficient continuation scheme based on shooting and pseudo-arc length continuation for undamped, unforced systems. Later, Sracic & Allen [43] implemented a similar approach for a damped, harmonically forced nonlinear system. This paper extends those approaches to deal with hysteretic systems in which the joint is modeled by many Jenkins sliders, whose dynamics are highly discontinuous.

A typical shooting method, such as that in [42], cannot be directly applied to a system with an Iwan joint. Those algorithms all assume that the nonlinear force in the system can be written as a function of the states, i.e. for an SDOF system $f_{nl} = f_{nl}(x, \dot{x})$. However, if the nonlinearity comes from an Iwan joint, then one must also consider the state of all of the sliders (i.e. as shown in Fig. 1) used to model the joint both at the current and previous timesteps so that $f_{nl} = f_{nl}(x(t), \dot{x}(t), \mathbf{y}(t), \mathbf{y}(t-\Delta t))$ where $\mathbf{y}$ typically includes 30–200 sliders. Such a large number of nonlinear states make methods such as that in [42] impractical, and even if computational resources were available, the hysteretic and discontinuous nature of the slider states cannot be directly included in that framework. This paper takes a closer look at the position or "state of sliders" in a typical vibration response and shows that they indeed play a critical role in the nonlinear behavior of the structure. We first show that the "reversal points", $\mathbf{x}_{rev}$, or points where the velocity of the system is zero, can be used to find the initial state of sliders; for weak nonlinearities only two reversal points are needed. Then, a simple quasi-static algorithm is proposed to evaluate the initial state of the sliders based on the reversal points, so one need only add a few reversal points $\mathbf{x}_{rev}$ to the continuation algorithm rather than all of the slider states $\mathbf{y}$, and the slider states can be found as a function of this much smaller set of variables $\mathbf{x}_{rev}$, i.e. we show that $\mathbf{y} \approx \mathbf{y}(\mathbf{x}_{rev})$. The proposed method is dubbed "Hysteresis Identification via Reversal Points or (HIRP)".

As in the continuation method presented in [42,43], in the continuation scheme developed in this work, the finite difference method is used to compute the Jacobians. It is shown that the finite difference step-size has a significant effect on the computational cost and also the efficiency of the proposed method. Accordingly, an algorithm is developed which can assess the optimum step-size for the different forcing frequencies. This achieves a higher computational efficiency.

To evaluate the efficacy of the proposed approach for realistic structures, a multi-DOF system with several joints, each modeled by an Iwan element with several Coulomb sliders, was investigated in this paper. The algorithm was used to compute the forced steady-state response for a range of forcing frequencies and amplitudes. Then, in order to test the feasibility of the proposed algorithm for larger finite element models, a 54 DOF model of the S4 Beam [8,33] was also investigated and the steady-state response was computed near one of the resonances for different force amplitudes.

2. Background

An Iwan element [4] describes a general hysteretic system created by an arrangement of n_s ideal elasto-plastic elements (i.e. Jenkins elements). These Jenkins elements are assumed to have the same elastic stiffness, i.e. $k = K/n_s$, but different strengths, i.e. f_i^*. The strength of the slider i, f_i^*, is defined as the allowable force that can be applied on the Jenkins element i before its slider starts to slip. If the force F applied on a system (represented by an Iwan element) is such that the loading on every Jenkins element is smaller than their corresponding strength, the element behaves like a linear spring with the stiffness equivalent to $K = (n_s)k$. However, if the load on any of Jenkins elements is larger than f_i^*, some sliders will slip and the joint force becomes a nonlinear function of the displacement. The force–displacement relation for the entire system can be defined as the sum of the strengths of the slipping sliders and the elastic force of the sliders that are stuck. The distribution of the strength between the sliders plays an important role in the behavior of the joint. In [4] the strength of each element is defined based on a density or distribution function, $\rho(f^*)$. The distribution function (DF) is the main core of any Iwan joint; two Iwan elements with the same stiffness but different distribution functions will show the same linear behavior but different nonlinear behaviors over a cycle.

One well known distribution function is that presented by Segalman in [6]. Segalman suggested to remove the stiffness, k, from the equations and instead parameterized the joint in terms of the maximum displacement of each spring,

$$\phi_i = f_i^*/k_i; \tag{1}$$

where ϕ_i is the maximum extension of the ith spring. While Iwan assumed a step function for the DF in [4], Segalman used a power-law distribution in [6] to represent the fact that the energy dissipation in bolted joints in the micro-slip regime is often observed to depend in an exponential fashion on the displacement,

$$\rho(\phi) = R\phi^{\chi}\left[H(\phi) - H(\phi - \phi_{\max})\right] + S\delta(\phi - \phi_{\max}), \tag{2}$$

where ϕ_{max} is the displacement at which all sliders slip, S is the slope of the force–displacement curve just before macro-slip, and R and χ define the strength and slope of the power-law energy dissipation.

The force in the Iwan element can be computed based on the position of sliders. The force of each Jenkins element is simply the force in each spring, or the spring stiffness times the deflection of the spring, which is related to the deflection of the joint $x_j(t)$ and the position of the slider, i.e. $f_{j,i} = k_i\left[x_j(t) - y_i(\phi, t)\right]$, where $y_i(\phi, t)$ is the position of slider i. Therefore, the total force in the jth Iwan joint is the sum of the elastic forces in the Jenkins elements [6],

$$f_j(t) = \int_0^{\infty} \left[x_j(t) - y(\phi, t)\right]\rho(\phi)d\phi \tag{3}$$

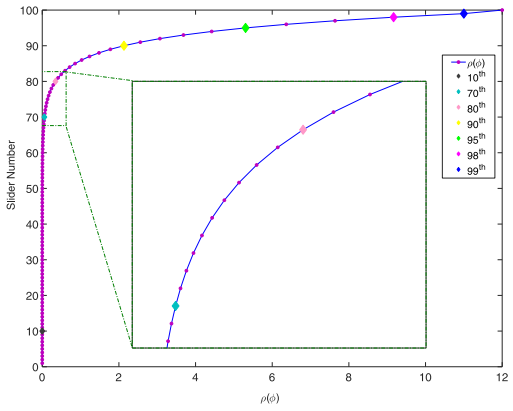

(a) $\rho(\phi)$: the distribution of sliders

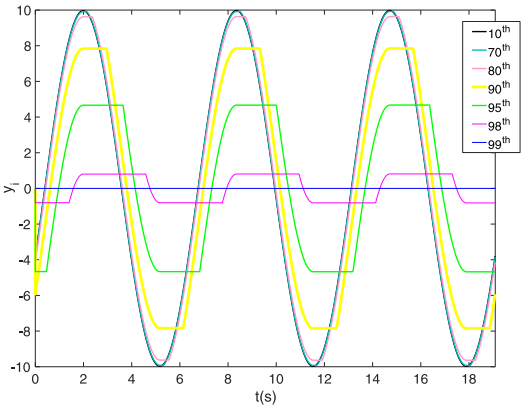

(b) Time response of some sliders

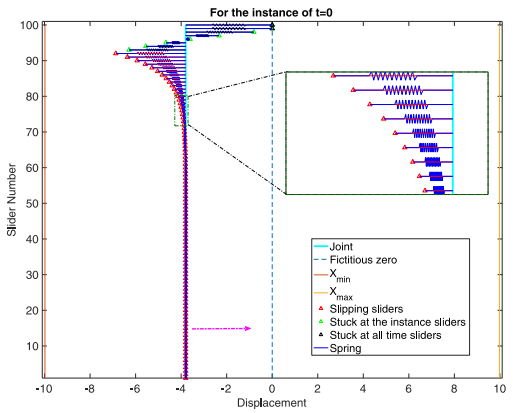

(c) $\mathbf{y}(0)$: Initial state of sliders

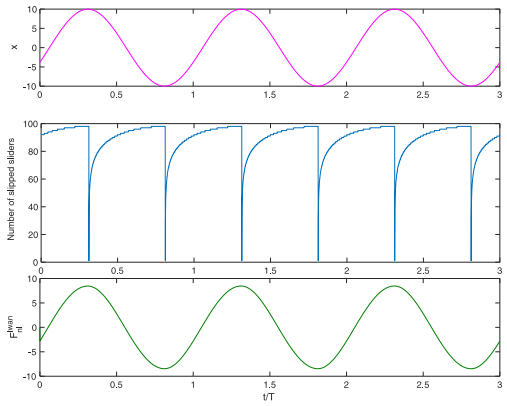

(d) x: displacement of joint, nonlinear force of the joint and number of slipped sliders

Fig. 2. The distribution of ϕ based on four-parameters Iwan presented in [6] and also the time response of 10th, 70th, 80th, 90th, 95th, 98th and 99th slider of an Iwan element with 100 sliders. (For interpretation of the references to color in this figure legend, the reader is referred to the web version of this article.)

This force can be incorporated into the equation of motion for a structural dynamic system with n DOF,

$$\mathbf{M}\ddot{\mathbf{x}}(t) + \mathbf{C}\dot{\mathbf{x}}(t) + \mathbf{K}\mathbf{x}(t) + \mathbf{f}_{nl}(\mathbf{x},\mathbf{y}) = \mathbf{F}_{ext}(t) \tag{4}$$

where $\mathbf{x}(t) = \left[x_1(t),\ldots,x_m(t)\right]^T$, $\dot{\mathbf{x}}(t) = \left[\dot{x}_1(t),\ldots,\dot{x}_m(t)\right]^T$, $\ddot{\mathbf{x}}(t) = \left[\ddot{x}_1(t),\ldots,\ddot{x}_m(t)\right]^T$, $\mathbf{f}_{nl}(\mathbf{x},\mathbf{y})$ is the nonlinear force applied in the system because of the Iwan joints and $\mathbf{F}_{ext}(t)$ is the harmonic force. If the system has a single Iwan joint, then the force would be $\mathbf{f}_{nl}(\mathbf{x},\mathbf{y}) = [0,\ldots,0,1,-1,0,\ldots,0]^{\mathrm{T}} f_j$ with the 1 and -1 placed at the nodes on either end of the Iwan joint and the force only depends on the displacements of those same two nodes, i.e. $x_j = [0,\ldots,0,1,-1,0,\ldots,0]\mathbf{x}$ is used in Eq. (3).

3. State of sliders

A periodic solution of Eq. (4) is obtained when $\mathbf{x}(t+T) = \mathbf{x}(t)$ and $\dot{\mathbf{x}}(t+T) = \dot{\mathbf{x}}(t)$, i.e. when the initial condition is chosen to match the state after one cycle of the forcing. A shooting function is defined, which can be minimized to find the periodic solutions for a range of forcing frequencies,

$$\mathbf{H}(\mathbf{z}_0,T) = \mathbf{z}_T(\mathbf{z}_0,T) - \mathbf{z}_0 \tag{5}$$

where $\mathbf{z}$ is a state variable vector, i.e. $\mathbf{z}(t) = \left[\mathbf{x}(t)^T, \dot{\mathbf{x}}(t)^T\right]^T$, $\mathbf{z}(0) = \mathbf{z}_0$ is the initial condition, T is the period of the applied harmonic force and $\mathbf{z}_T$ is the response of the system after one period, calculated by integrating the differential equation in Eq. (4).

For a system to show steady-state behavior, all of the terms in Eq. (4) must be periodic. If the displacement is periodic then the inertial, damping and stiffness forces will also be periodic, and so the nonlinear force due to the Coulomb sliders must also be periodic for the equation to be balanced. While we have not presented a rigorous proof, we assert that this will only be the case if the states of all of the sliders $y(\phi,t)$ in Eq. (3) are also be periodic.

To illustrate this, a SDOF system was simulated which contains an Iwan joint comprised of one hundred sliders. This hysteretic system is excited by a harmonic force over three periods and the results are plotted in Fig. 2 after the system has reached its steady-state condition. It can be observed that the force and the number of slipping sliders at each instant are also periodic. For example, the number of slipped sliders is identical (91 sliders) for $t = 0$, T, $2T$ and $3T$, as shown in Fig. 2d. Fig. 2a shows the distribution of slider strengths based on ϕ, defined in Eq. (2), and discretized to represent the joint with 100 sliders of strengths ϕ_i. The displacements of the seven sliders shown by "diamonds" are shown in Fig. 2b over three periods. As can be seen in Fig. 2b, the sliders' response becomes more nonlinear as their ϕ_i value becomes larger; the first slider slips continuously over one period while the 98th slider sticks and slips periodically. It is also interesting to note that each slider slips at a displacement equal to ϕ_i, given by the horizontal axis of Fig. 2a. Most importantly, the motion of the sliders is periodic, i.e. $\mathbf{y}(t+nT) = \mathbf{y}(t)$ where $\mathbf{y}(t) = [y_1(t), \ldots, y_{ns}(t)]^T$ is the vector of the state (position) of each slider and the initial state of the sliders at $t = 0$, i.e. $\mathbf{y}(0) = [y_1(0), y_2(0), \ldots, y_{ns}(0)]^T$, must be known in order to evaluate $\mathbf{f}_{nl}(t_1 > 0)$ and so on. It will be helpful in the algorithm that follows to define a shooting function that goes to zero when the slider states are periodic, and which is given below.

$$\frac{\|\mathbf{H}_{\mathbf{y}}(\mathbf{y}(0), T)\|}{\|\mathbf{y}(0)\|} = \frac{\|\mathbf{y}(T) - \mathbf{y}(0)\|}{\|\mathbf{y}(0)\|} < \epsilon_y \tag{6}$$

In order to calculate the Jacobian matrix, the integration will be performed for every state variable. If one were to add the initial state of all of the sliders to the state vector, assuming that each integration takes m seconds, the total cost of each Jacobian matrix would be $[2 \times (\text{number of DoF}) + \text{number of sliders} + 1]m$ seconds. Since 50 to 150 sliders are typically needed to capture the stick–slip transition accurately, this would make the continuation scheme extremely expensive. Furthermore, the slider states are highly discontinuous, as seen in Fig. 2b, so it is challenging to compute their derivatives numerically. Hence, it is crucial to find another way of considering the effect of $\mathbf{y}(0)$ in the problem while maintaining the efficiency of the algorithm. Fortunately, the following section will show that it is not necessary to track all n_s slider states in the continuation, but that the vector $\mathbf{y}(0)$ can be found by augmenting $\mathbf{x}_0$ and $\dot{\mathbf{x}}_0$ with a few additional variables, namely, with the displacement at the past reversal point(s).

3.1. Reversal points

The ith slider will slip at t_{m+1} if $\phi_i \geq x(t_{m+1}) - y_i(t_m)$ when the spring has reached to its maximum extension and the force applied on the sliders is larger than the strength of slider, i.e. $f_i^* > \mu N = k\phi_i$. This criteria can be implemented to divide the sliders into two main groups:

Stuck at all time instants, S1. Some sliders never slip over a cycle shown by the black triangles in the figures of this paper and also are dubbed as "stuck at all times". That is because their maximum extension is larger than max displacement of the joint during that time response. In other words, the normal force in these Jenkins elements is large enough so that they can stretch to from one reversal point to another without slipping. Hence, the slider position is zero over a cycle (i.e. $y_i(t) = 0,\ 0 \leq t \leq T$). The 99th slider in Fig. 2b is an example of an S1 slider.

Stick and slip periodically, S2. Sliders that will slip and stick periodically and are shown by green and red triangles in Fig. 2c and elsewhere. For example, the 10th to 98th sliders in Fig. 2b show both stick and slip to varying degrees. Moreover, the slipping sliders follow the joint with a certain extension in the spring equal to ϕ_i, and have the same velocity as the joint. This is because the sliders slip when the spring has extended to its maximum value ϕ_i as can be seen for the 1st to 3rd sliders in Fig. 3d, as discussed below.

To further illustrate the state of the sliders at each instant, and to help to explain the proposed algorithm, Fig. 3 shows the slider states for an SDOF system with an Iwan joint, highlighting six different instants during one cycle of vibration. The joint is shown by a cyan vertical line, the sliders are shown with the triangles and the dashed vertical line represents the original equilibrium position of all of the sliders; any slider that does not slip at all over a period will remain at the equilibrium position. The positions of the slipping sliders are shown by red triangles and the green triangles denote those that slip at some point during the period but are stuck at the instant of interest. The state of each slider, y_i, can be defined as the distance between the current position of the slider and the original equilibrium position of the joint, as shown in Fig. 3a.

In Figs. 3a and 3b, the joint is moving toward x_{min} and the 1st to 8th sliders are slipping and following the joint by an offset in displacement equal to ϕ_i. This happens because $f_i^* = \mu N = k\phi_i$ where f_i^* is the friction force and N is the normal force. Fig. 3c shows the state when the joint reaches x_{min} and $\dot{x} = 0$. At this reversal point, all of the sliders become stuck. Mathematically, all "S1" sliders are at the equilibrium position $y_i = 0$ whereas the "S2" sliders now have $y_i = x_{rev}^1 + \phi_i$ where $x_{rev}^1 = x_{min}$. This illustrates how the reversal points can be used to construct the slider positions at any instant, and hence the initial slider positions, $\mathbf{y}(0)$, which are needed to initiate the shooting algorithm. This is one of the main ideas behind the algorithm proposed in this paper.

3.1.1. Reversal points and state of sliders

The example in Section 3.1 has just illustrated that the states of sliders and the nonlinear force of the joint are history-dependent; they depend on any past reversals of the joint. To better understand this, it is advantageous to explore how sliders' positions evolve from one reversal point to another. Figs. 3c to 3f show the evolution of the states of the sliders from x_{min} to x_{max} at six different instants. The sliders are first stuck at ($x_{min} + \phi_i$,i=1, …,8) in Fig. 3c and the joint then starts to move toward x_{max} and compresses the springs attached to each slider. Notice that the joint must move $2\phi_i$ before the each slider will slip; moving from 0 to ϕ_i brings the spring to its equilibrium position, and then moving by an additional ϕ_i brings the spring to its maximal extension. The sliders start to slip from the weakest to the strongest. Since the joint velocity has an identical sign between the two reversal points:

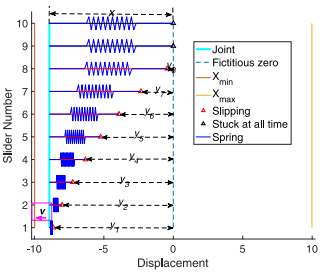

(a) When $x_{min} < x < 0$ and $\dot{x} < 0$, the 1^{th} to 8^{th} sliders are sliding and the 9^{th} and 10^{th} sliders are stuck at equilibrium.

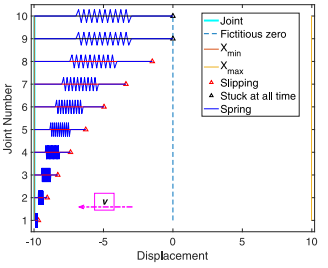

(b) One moment before $x = x_{min}$. When $x \approx x_{min}$ with negative velocity $\dot{x} < 0$. The 1^{th} to 8^{th} sliders are sliding. The sliders 9^{th} and 10^{th} remain stuck at equilibrium.

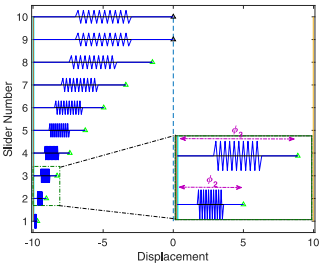

(c) At the turning point, where $x = x_{min}$ and, $\dot{x} = 0$. The 1^{st} to 8^{th} sliders are now stuck at $(x_{min} + \phi_i)$, the positions shown with green triangles. The 9^{th} and 10^{th} sliders remain stuck at equilibrium.

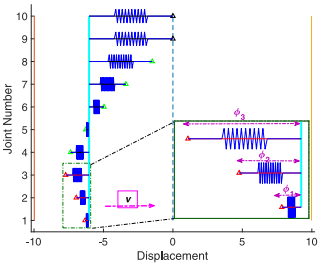

(d) Additional sliders slip the displacement progresses. At the instant shown the 1^{st} to 3^{th} sliders are slipping, i.e $y_i = x(t) - \phi_i$, and the 4^{th} to 8^{th} sliders are still stuck at $(x_{min} + \phi_i)$.

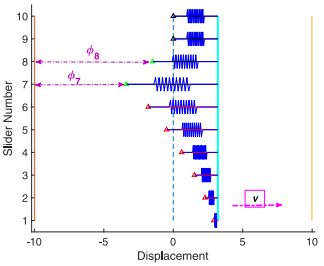

(e) Additional sliders slip the displacement progresses. At the instant shown the 1^{st} to 6^{th} sliders are slipping, i.e $y_i = x(t) - \phi_i$, and the 7^{th} and 8^{th} sliders are still stuck at $(x_{min} + \phi_i)$.

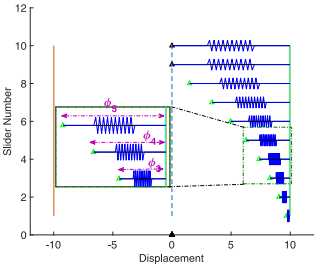

(f) At the turning point, where $x = x_{max}$ and, $\dot{x} = 0$. The 1^{st} to 8^{th} sliders are now stuck at $(x_{max} - \phi_i)$ and the 9^{th} and 10^{th} slider remain stuck at equilibrium.

Fig. 3. Illustration of the state of the Iwan sliders at different time instants during a cycle of vibration. (For interpretation of the references to color in this figure legend, the reader is referred to the web version of this article.)

- If the state of a slider is known at one reversal point, one can find the state of that slider at the next reversal points based on its strength. Specifically, assuming that x_{rev}^m is the mth reversal point, to determine if a slider has slipped at the $m+1$th reversal point, ϕ_i is compared with $\left[x_{rev}^{m+1} - y_i(x_{rev}^m)\right]$ and if ϕ_i is larger, the slider is slipping and hence it will follow the joint with an offset in the displacement equal to ϕ_i. Otherwise, it will remain at the state it had at the previous reversal point, i.e. $y_i(x_{rev}^m)$:

$$y_i(x_{rev}^{m+1}) = \begin{cases} y_i(x_{rev}^m), & \text{if } \phi_i > \left|x_{rev}^{m+1} - y_i(x_{rev}^m)\right| \\ x_{rev}^{m+1} - \text{sign}(\dot{x}(x_{rev}^m(+)))\ \phi_i, & \text{otherwise} \end{cases} \tag{7}$$

Each slider follows the displacement x, so the term $\text{sign}(\dot{x}(x_{rev}^m(+)))$ is introduced where the notation $\dot{x}(x_{rev}^m(+))$ denotes the velocity just after x_{rev}^m; the sign of the velocity is the same from x_{rev}^m to x_{rev}^{m+1}.

One can use the same approach to compute the state of the ith slider, $y_i(t)$, at any instant in time after the latest reversal. Indeed, if the state of sliders is known at the reversal point x_{rev}^m, the state of sliders at any instant between x_{rev}^m and x_{rev}^{m+1} can be calculated. For example, if t is a time instant when the joint position is between x_{rev}^m and x_{rev}^{m+1}, the state of sliders at t can be calculated as:

$$y_i(t) = \begin{cases} y_i(x_{rev}^m), & \text{if } \phi_i > \left|x(t) - y_i(x_{rev}^m)\right| \\ x(t) - \text{sign}(\dot{x}(x_{rev}^m(+)))\ \phi_i, & \text{otherwise} \end{cases} \tag{8}$$

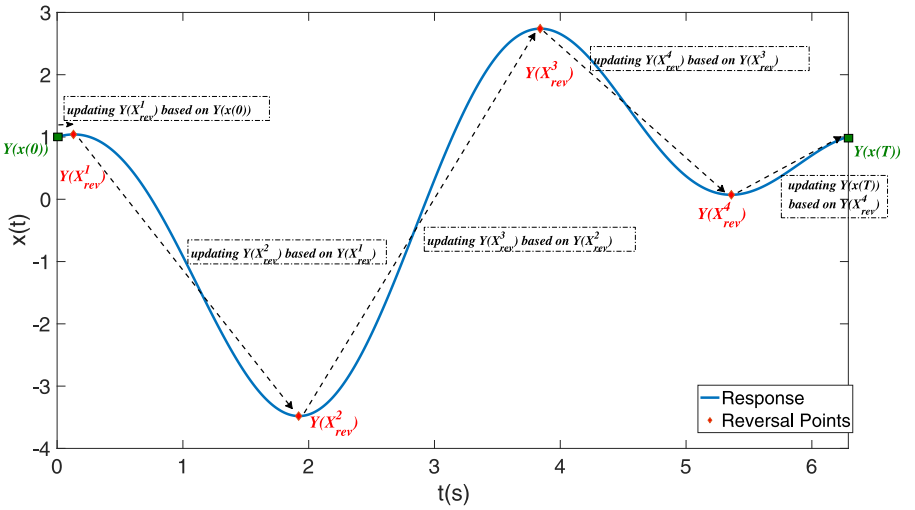

Fig. 4. Example time history where the slider position algorithm is used to update the positions of the sliders from $\mathbf{y}(0)$ to $\mathbf{y}(T)$.

In the continuation algorithm presented here, the slider states are known at the initial state $y_i(0)$ and $y_i(t)$ is desired, so one can start with $y_i(0)$ and calculate $y_i(x^1_{rev})$, $y_i(x^2_{rev})$, ... up until the last reversal point right before t and finally predict $y_i(t)$ based on Eq. (8). This idea is used to develop the proposed quasi-static algorithm in the following section.

3.2. Evaluation of the initial state of sliders

Using the developments in the previous section, the initial state of the sliders is found using the following algorithm. This assumes that one has an estimate for x^m_{rev}, i.e. from a previous iteration of the continuation procedure.

- 1- Start with all sliders at rest at $t = 0$ for iteration $k = 0$ so $\mathbf{y}^k(0) = [0, \ldots, 0]$.
- 2- Calculate the state of sliders at reversal points 1 through m using Eq. (7), where m is the last reversal point before $t = T$.
- 3- Use that result and Eq. (8) to find the state of the sliders at $t = T$.
- 4- Evaluate Eq. (6). If the criteria is not met go back to the second step, increment the iteration number k, assume that $(\mathbf{y}^k(0) = \mathbf{y}^{k-1}(T))$ and repeat the process. Otherwise, use the states $\mathbf{y}^k(T)$ obtained as the initial states and proceed to integrate the equation of motion over one period.

Fig. 4 illustrates the algorithm for an Iwan joint with 5 sliders whose parameters are defined in Table 1, and which oscillates over one period. Three iterations are needed in order to calculate $\mathbf{y}(0)$, and the iterations are shown in Tables 2 to 4. The algorithm begins by assuming that all of the slider positions are zero and so uses Eq. (7) with $y_i(0) = 0$ to assign the slider positions at x^1_{rev}. Specifically, any slider for which $\phi_i < x^1_{rev}$, or whose maximum extension has been exceeded by x^1_{rev}, will slip and so its position $y_i(x^1_{rev})$ must be updated. For the case illustrated in Fig. 4, and using the slider properties in Table 1, only the first slider will slip at x^1_{rev}, so at this reversal point we find $y_1(x^1_{rev}) = x^1_{rev} - \phi_i \text{sign}\left(\dot{x}(x^m_{rev}(+))\right) = 1.04 - 0.38 = 0.66$ and $y_i(x^1_{rev}) = 0$ for $i = 2, 3, 4, 5$. Notice that what should be compared with ϕ_i is the relative displacement from the last stuck position of the slider and the current position of joint. Proceeding to the second reversal point, we calculate $\left|x^2_{rev} - y_i(x^1_{rev})\right|$, which is $|-3.48 - .66|$ for the first slider and simply 3.48 for the rest of the sliders. Hence at x^2_{rev} all sliders have slipped except for the 5th. The same procedure can then be used to go from the 2nd reversal point to the 3rd and 4th, and the result is shown in Table 2.

Now that the slider states are known at the last reversal point, we can proceed to calculate them at the end of the period, $\mathbf{y}^0(T)$, using the same procedure. The last part of the first iteration will calculate $\mathbf{y}^0(T)$ based on Eq. (8). For example for the case of the Iwan joint with the five sliders shown in Table 2, the 1st to 3rd sliders are slipping while the 4th slider is stuck in its original position. The state of sliders after the zeroth iteration, $\mathbf{y}^0(T)$ is given in the last column in Table 2. If the response is to be periodic, then this should match the slider states at time zero, and so Eq. (6) is used to check whether this has been satisfied to the required tolerance. If the criteria is not met, the algorithm will be repeated again, but this time it will start with $\mathbf{y}^1(0) = \mathbf{y}^0(T)$ obtained from the first iteration as the initial guess. For the example shown in Table 2, it can be seen that the criteria in Eq. (6) is not met. Therefore, the algorithm continues to the second iteration. Table 3, shows the second iteration of the algorithm and Table 4 shows the third and since $\mathbf{y}^2(T) = \mathbf{y}^2(0)$ the algorithm terminates.

3.3. Nonlinear force

Implicit integration schemes such as Newmark-Beta have been implemented to compute the dynamic response of frictional systems modeled with Coulomb sliders and are also applicable to Iwan elements. The algorithm proposed in this paper computes the

Table 1
Specification for the example of a SDOF system with an Iwan joint described by five sliders. ϕ: the strength of the sliders, x_{rev}: the reversal points over the period shown in Fig. 4.

Slider	ϕ	Reversal point	x_{rev}
1st	0.38	1	1.04
2nd	1.22	2	−3.48
3rd	2.23	3	2.74
4th	3.44	4	0.072
5th	4.10		

Table 2
The first iteration of the algorithm used to find the initial slider positions, applied to the system in Table 1 whose response is shown in Fig. 4.

Iteration: 1		Update $\mathbf{y}^0$ at each reversal point				Find $\mathbf{y}^0(T)$		
Slider	$\mathbf{y}^0(0)$	$\mathbf{y}^0(x^1_{rev})$	$\mathbf{y}^0(x^2_{rev})$	$\mathbf{y}^0(x^3_{rev})$	$\mathbf{y}^0(x^4_{rev})$	Displacement	Slipping?	$y^0(T)$
1	0	$x^1_{rev}-\phi_1$	$x^2_{rev}+\phi_1$	$x^3_{rev}-\phi_1$	$x^4_{rev}+\phi_1$	$x(T)-\mathbf{y}^0(x^4_{rev})$	Yes	$x_0-\phi_1$
2	0	0	$x^2_{rev}+\phi_2$	$x^3_{rev}-\phi_2$	$x^4_{rev}+\phi_2$	$x(T)-\mathbf{y}^0(x^4_{rev})$	Yes	$x_0-\phi_2$
3	0	0	$x^2_{rev}+\phi_3$	$x^3_{rev}-\phi_3$	$x^3_{rev}-\phi_3$	$x(T)-\mathbf{y}^0(x^4_{rev})$	Yes	$x_0-\phi_3$
4	0	0	$x^2_{rev}+\phi_4$	$x^3_{rev}-\phi_4$	$x^3_{rev}-\phi_4$	$x(T)-\mathbf{y}^0(x^4_{rev})$	No	$x^3_{rev}-\phi_4$
5	0	0	0	0	0	0	Never	0

Table 3
The second iteration of the algorithm used to find the initial slider positions.

Iteration: 2		Update $\mathbf{y}^0$ at each reversal point		Find $\mathbf{y}^0(T)$		
Slider	$\mathbf{y}^1(0)=\mathbf{y}^0(T)$	...	$\mathbf{y}^1(x^4_{rev})$	Displacement	Slipping?	$\mathbf{y}^1(T)$
1	$x_0-\phi_1$	...	$x^4_{rev}+\phi_1$	$x(T)-\mathbf{y}^1(x^4_{rev})$	Yes	$x_0-\phi_1$
2	$x_0-\phi_2$	...	$x^4_{rev}+\phi_2$	$x(T)-\mathbf{y}^1(x^4_{rev})$	No	$x^4_{rev}+\phi_2$
3	$x_0-\phi_3$	...	$x^3_{rev}-\phi_3$	$x(T)-\mathbf{y}^1(x^4_{rev})$	No	$x^3_{rev}-\phi_3$
4	$x^3_{rev}-\phi_4$	...	$x^3_{rev}-\phi_4$	$x(T)-\mathbf{y}^1(x^4_{rev})$	No	$x^3_{rev}-\phi_4$
5	0	...	0		Never	0

Table 4
The third and final iteration of the algorithm used to find the initial slider positions.

Iteration: 3		Update $\mathbf{y}^0$ at each reversal point		Find $\mathbf{y}^0(T)$		
Slider	$\mathbf{y}^2(0)=\mathbf{y}^1(T)$	...	$\mathbf{y}^2(x^4_{rev})$	Displacement	Slipping?	$\mathbf{y}^2(T)$
1	$x_0-\phi_1$	...	$x^4_{rev}+\phi_1$	$x(T)-\mathbf{y}^2(x^4_{rev})$	Yes	$x_0-\phi_1$
2	$x^4_{rev}+\phi_2$	...	$x^4_{rev}+\phi_2$	$x(T)-\mathbf{y}^2(x^4_{rev})$	No	$x^4_{rev}+\phi_2$
3	$x^3_{rev}-\phi_3$	...	$x^3_{rev}-\phi_3$	$x(T)-\mathbf{y}^2(x^4_{rev})$	No	$x^3_{rev}-\phi_3$
4	$x^3_{rev}-\phi_4$	...	$x^3_{rev}-\phi_4$	$x(T)-\mathbf{y}^2(x^4_{rev})$	No	$x^3_{rev}-\phi_4$
5	0	...	0		Never	0

initial state of the sliders, which is then provided to the Newmark-Beta algorithm, along with the initial displacement and velocity of the system, and the nonlinear force and stiffness can be calculated using the difference between the current position of joint and the previous state of sliders based on Eq. (3). In this work, the discretization method presented in [6] is implemented to convert the integral in Eq. (3) over $(0,\phi_{max})$ into a sum over N intervals. Using the geometric series approach in [6], the force in the jth Iwan joint at time t becomes:

$$f_j(t)=\sum_{i=1}^{N} f_{ji}(t)+F_\delta(t) \tag{9}$$

where $f_{ji}(t)$ is the force of the slider i at time t and F_δ is the dirac delta part of $\rho(\phi)$. It should be clarified that $f_{ji}(t)$ is different than the strength, ϕ_i, of slider i and is defined as:

$$f_{ji}(t)=\begin{cases} R\frac{\phi_{r,i}^{2+\chi}-\phi_{l,i}^{2+\chi}}{2+\chi} sgn\left[x(t)-y_i(t)\right] & \left[x(t)-y_i(t)\right]=\phi_i \\ R\frac{\phi_{r,i}^{1+\chi}-\phi_{l,i}^{1+\chi}}{1+\chi}\left[x(t)-y_i(t)\right] & \left[x(t)-y_i(t)\right]<\phi_i \end{cases} \tag{10}$$

where $\phi_{r,i}$ and $\phi_{l,i}$ are the coordinates of the left and right hand of each subinterval, $\Delta\phi_i$, where $\sum_{i=1}^{N}\Delta\phi_i=\phi_{max}$ [6]. In the above equation, the top term is for the sliders that are slipping and so the force is at its maximum value for each slider and the bottom

term is for those that are stuck. The force of the strongest slider F_δ is defined as below:

$$F_\delta = S\phi_{max}\left[x(t) - y_\delta(t)\right] \tag{11}$$

For more details in this regard see [6]. Finally, the discretized equation for the stiffness of the jth Iwan joint in the micro-slip regime can be defined as:

$$k_j(x(t)) = \frac{\mathrm{d}F(t)}{\mathrm{d}x} = \sum_{i=1}^{N} K_{ji}(t) + S \tag{12}$$

where

$$K_{ji}(t) = \begin{cases} 0 & \left[x(t) - y_i(t)\right] = \phi_i \\ R\frac{\phi_{r,i}^{1+\chi} - \phi_{l,i}^{1+\chi}}{1+\chi} & \left[x(t) - y_i(t)\right] < \phi_i \end{cases} \tag{13}$$

With $K_{ji}(t)$ and $f_{ji}(t)$ defined based on the slider positions $\mathbf{y}(t)$ for each joint, given the initial conditions of the system the Newmark-Beta algorithm can be used to integrate the system in Eq. (4) over time. For example, given the initial state of sliders, i.e. $\mathbf{y}(0)$, the force at $t = 0$ in each joint can be calculated by using Eq. (9) and then the nonlinear force vector $\mathbf{f}_{nl}(\mathbf{x}(0), \mathbf{y}(0))$ can be assembled as discussed previously. Consequently, the initial acceleration is given by the following.

$$\ddot{\mathbf{x}}(0) = \mathbf{M}^{-1}\left[\mathbf{F}_{ext}(0) - \left[\mathbf{C}\dot{\mathbf{x}}(0) + \mathbf{K}\mathbf{x}(0) + \mathbf{f}_{nl}(\mathbf{x}(0), \mathbf{y}(0))\right]\right] \tag{14}$$

4. Computing nonlinear frequency response

4.1. Adapting time domain continuation to work with Iwan joints

As explained in Section 3, this paper proposes adding the reversal points as additional state variables so that the initial displacements of the sliders can be computed. Hence, the continuation method presented in [42,43] must be modified to check the periodicity of the added state variables, denoted $\mathbf{x}_{rev}$, to correct them in each iteration, and to predict them for the next frequency step. The additional state variables are added to the state vector so that the new initial state vector becomes:

$$\mathbf{z}_0 = \begin{bmatrix} \mathbf{x}_0 & \dot{\mathbf{x}}_0 & x_{1,rev}^1 & \dots & x_{1,rev}^{n_1} & \dots & x_{j,rev}^1 & \dots & x_{j,rev}^{n_j} & \dots \end{bmatrix}^T \tag{15}$$

where $x_{j,rev}^1$ denotes the first reversal point for the jth joint and the series continues until all joints have been accounted for. Note that the number, n_j and location (in time) of the reversal points may be different for each joint. It may appear that the state vector above mixes time instants, because it contains the state of the system at time zero as well as the reversal points, which happen at various times within a period. However, the reversal points are a surrogate for the initial slider states, and so the initial state vector does only describe the system at the initial time instant.

Following the approach in [43], a good starting guess for the state variables is supplied by the user (typically a low frequency or low amplitude solution for the underlying linear system). The quasi-static algorithm proposed in Section 3.2 is then used in order to evaluate the initial state of the sliders. Since the nonlinear force explained in Section 3.3 is history-dependent, an implicit integration scheme like the Newmark-β method [44] is needed in order to calculate the response of the system over one period. Inside the integration scheme, the algorithm iterates on the nonlinear force and stiffness until the response at the next time step has been computed to acceptable accuracy. After the integrating over a period, the shooting function, defined below, is checked to quantify the periodicity of $\mathbf{x}$, $\dot{\mathbf{x}}$ and the reversal points.

$$\mathbf{H}_{\mathbf{z}_0}(\mathbf{z}_0, T) = \mathbf{z}_T(\mathbf{z}_0, T) - \mathbf{z}_0 \tag{16}$$

where $\mathbf{z}_T(\mathbf{z}_0, T, x_{rev})$ is the state vector found by integrating until $t = T$. This is comprised of $\mathbf{x}(T)$, $\dot{\mathbf{x}}(T)$, the state of the system at $t = T$, and the reversal points $x_{j,rev}^n(T)$, which are computed by calculating the displacements across each Iwan joint x_j at $t = T$ and finding the local minima and maxima. In contrast $\mathbf{z}_0$ includes $x_{j,rev}^n(0)$, which are computed from the time history at a previous iteration and used to find the initial states of sliders. Consequently, the criteria for considering the solution converged becomes the following, which is identical to that used in [42,43] except that the definition of $\mathbf{z}_0$ has changed.

$$\frac{\|\mathbf{H}_{\mathbf{z}_0}(\mathbf{z}_0, T)\|}{\|\mathbf{z}_0\|} < \epsilon_s \tag{17}$$

where the shooting function tolerance ϵ_s is set at 10^{-6} for the results shown in this paper. Note that if Eq. (17) is satisfied, the initial slider states will also be periodic to a similar tolerance, and so it is not necessary to check Eq. (6) separately. If the criteria is not satisfied, a sequence of corrections is needed to correct $\mathbf{z}_0$ until the response becomes periodic. The Newton–Raphson procedure in [42,43] is used to find this solution, where the linear system below is inverted at each iteration to find a correction for the initial state $\Delta\mathbf{z}_0$ and period ΔT.

$$\begin{bmatrix} \frac{\partial \mathbf{H}_{\mathbf{z}_0}}{\partial \mathbf{z}_0}|_{(\mathbf{z}_0,T)} & \frac{\partial \mathbf{H}_{\mathbf{z}_0}}{\partial T}|_{(\mathbf{z}_0,T)} \end{bmatrix} \begin{bmatrix} \Delta\mathbf{z}_0 \\ \Delta T \end{bmatrix} = \begin{bmatrix} -\mathbf{H}_{\mathbf{z}_0}(\mathbf{z}_0, t = T) \\ 0 \end{bmatrix} \tag{18}$$

After finding the first solution for a frequency value well below the natural frequency of the system, continuation is used to find the whole branch of FRFs by marching along the FRF (e.g. in a direction of increasing frequency). Once a solution has been found, the pseudo-arclength method is used to predict the next solution. The prediction part consists of calculating the tangent vector $\mathbf{P}$ by finding the vector in the null space of the matrix below.

$$\left[\frac{\partial \mathbf{H}_{\mathbf{z}_0}}{\partial \mathbf{z}_0}|_{(\mathbf{z}_{0,j},T_j)} \qquad \frac{\partial \mathbf{H}_{\mathbf{z}_0}}{\partial T}|_{(\mathbf{z}_{0,j},T_j)}\right]\{\mathbf{P}_{(j)}\} = \begin{Bmatrix}\mathbf{0}\\0\end{Bmatrix} \tag{19}$$

where the subscript (j) denotes the jth converged solution for the frequency response and $\{\mathbf{P}_{(j)}\} = [\mathbf{P}^T_{\mathbf{z}_0,(j)} \quad P_{T,(j)}]^T$. Then, the desired tangent vector is used with a user-defined step-size s_j to predict the $(j+1)$th solution as $\mathbf{z}^{pr}_{0,(j+1)} = \mathbf{z}_{0,(j)} + s_j\mathbf{P}_{\mathbf{z}_0,(j)}$ and $T^{pr}{}_{(j+1)} = T_j + s_j P_{T,(j)}$. Then, the predicted values are used as the first guess for another round of Newton–Raphson iterations to find the converged solution. This correction step iterates on the values for $\mathbf{z}^j_0$ and T^j using the linear system of equations below until the convergence in Eq. (17) is met.

$$\begin{bmatrix}\frac{\partial \mathbf{H}_{\mathbf{z}_0}}{\partial \mathbf{z}_0}|_{(\mathbf{z}^k_{0,j+1},T^k_{j+1})} & \frac{\partial \mathbf{H}_{\mathbf{z}_0}}{\partial T}|_{(\mathbf{z}^k_{0,j+1},T^k_{j+1})}\\ \mathbf{P}^T_{\mathbf{z}_0,(j)} & P_{T,(j)}\end{bmatrix}\begin{bmatrix}\Delta\mathbf{z}^k_{0,j+1}\\ \Delta T^k_{j+1}\end{bmatrix} = \begin{bmatrix}-\mathbf{H}_{\mathbf{z}_0}(\mathbf{z}^k_{0,j+1},T^k_{j+1})\\0\\0\end{bmatrix} \tag{20}$$

Note that in this step the corrections are forced to be perpendicular to the prediction, as done in [42,43]. This tends to improve convergence of these correction steps. Continuing in this way, the whole branch of solutions for a range of forcing frequency can obtained.

4.2. Finite difference derivatives

In order to calculate the Jacobians in Eqs. (18), (19) and (20), this work follows [43] using the finite difference method. To do this, the user must define step sizes ϵ_z and ϵ_T, are used and the equation of motion is integrated over a period for the incremented initial conditions, $\mathbf{z}_0 + \mathbf{e}_n\epsilon_z$ and $T + \epsilon_T$, where $\mathbf{e}_n$ is a vector of zeros with a value of unity in the state of interest. Denoting the perturbed state-variables obtained after integration as i.e. $\mathbf{z}_{0,(p)}$, the finite difference derivative with respect to the period T is

$$\frac{\mathrm{d}\mathbf{H}_{\mathbf{z}_0}}{\mathrm{d}T} = \frac{\mathbf{z}_{0,(p)} - \mathbf{z}_0}{\epsilon_T} \tag{21}$$

and the nth column of $\frac{\partial \mathbf{H}_{\mathbf{z}_0}}{\partial \mathbf{z}_0}$ can be calculated as:

$$\frac{\mathrm{d}\mathbf{H}_{\mathbf{z}_0}}{\mathrm{d}z_{0,n}} = \frac{\mathbf{z}_{0,(p)} - \mathbf{z}_0}{\epsilon_z} \tag{22}$$

where $z_{0,n}$ is the nth element of the state vector. The finite difference step-size value plays an important role in the efficiency and also the computational cost of the problem. In general, using smaller finite difference step-sizes leads to more accurate results but increases the computational cost. However, if the step-size is too small, computational noise may cause a loss in accuracy. Hence, the finite difference step-size may need to be adapted at each frequency line. For example, at the turning points near resonance, the response amplitude is much larger so the computational noise may increase, yet the function changes quickly requiring smaller step sizes. To address this, the following algorithm was developed.

4.2.1. An algorithm for the finite difference step-size

The algorithm shown in Fig. 5 was developed to assure that accurate finite difference derivatives could be computed. This algorithm starts with a user specified value for s_f and then uses $\epsilon_z = 10^{(s_f)}$. Then, the progress of the Newton–Raphson iterations is tracked as the shooting function is minimized. If the shooting function falls below the specified tolerance then the stepsize is left unchanged. It calculates the shooting function for each iteration of the main algorithm until the value of the shooting function becomes either less than the specified tolerance or larger than the error of the previous iteration.

In contrast, if the value of the shooting function increases compared to the previous iteration, then the stepsize will be updated. The average of the error is calculated over all the iterations that used s^0_f and stored in *Ave* in Fig. 5. Then, $s^+_f = s^0_f + 1$ and $s^-_f = s^0_f - 1$ are specified. The algorithm will iterate for N_{ss} times specified by user ($N_{ss} = 5$ in this work) and the shooting function is calculated for each of them. The average error over those N_{ss} iterations is computed and denoted $E(s^+_f)$ and $E(s^-_f)$. Finally, the smallest value between $E(s^+_f)$, $E(s^0_f)$ and $E(s^-_f)$ is chosen and s_f corresponding to that value is selected as the step-size ($\epsilon_z = 10^{s_f}$) for the next iterations. The Newton–Raphson iterations then continue with the selected step-size until either the error in the shooting function falls below the tolerance or again begins to increase.

4.3. Jacobian computation

The Jacobian matrix must be calculated many times during the continuation scheme, for example for each correction or prediction step in Eq. (18) or (19). The Jacobian matrix is calculated column by column, and each column requires integrating the system over a period with one of the state variables perturbed while the others are remain unchanged. So, for the case of Jacobian matrix in Eq. (18), the integration must be performed $2 \times (\text{number of states}) + n_{rev} + 1$ times.

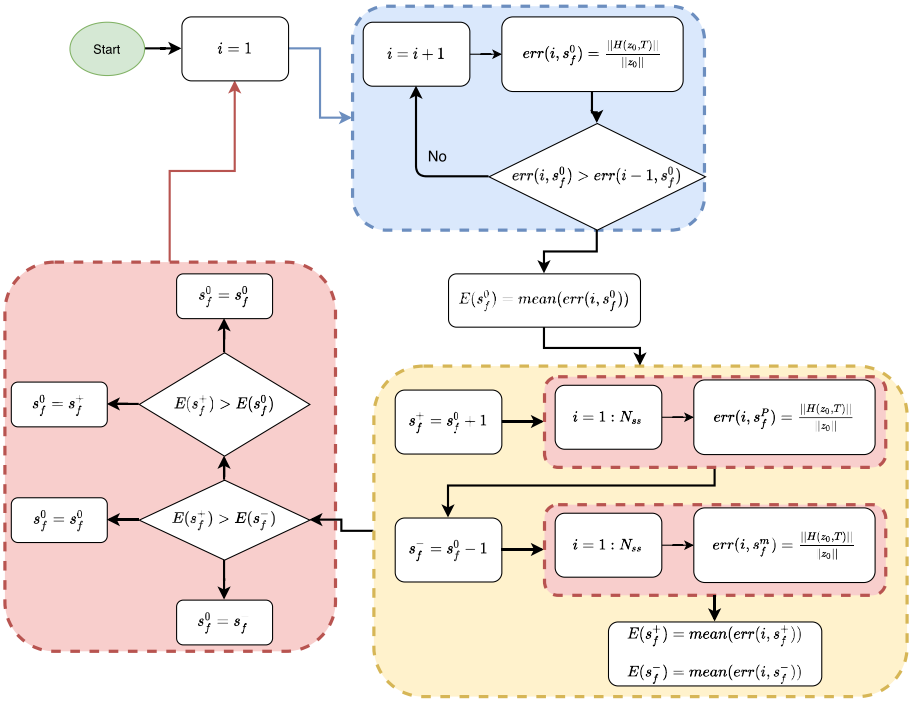

Fig. 5. The algorithm for the step-size.

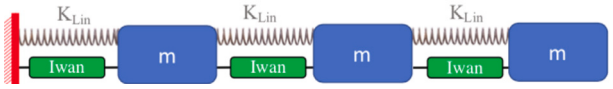

Fig. 6. Three DOF system with three Iwan joints.

In the proposed algorithm the number of reversal points is allowed to change from one iteration to the next, and so the size of the Jacobian matrix may change in each iteration. Fortunately, this can be dealt with by comparing any new reversal points with the initial position of the joint. Specifically, if in iteration i, the response shows a reversals, i.e. $x_{rev}^i = [x_{rev}^1, \dots, x_{rev}^a]$ and after the next iteration there are $a+b$ reversals, i.e. $x_{rev}^{i+1} = [x_{rev}^1, \dots, x_{rev}^{a+b}]$, then both iterations are treated as if they have $a+b$ reversal points and the additional reversal points are set to x_T, i.e. $x_{rev}^i = [x_{rev}^1, \dots, x_{rev}^a, x_T, \dots, x_T]$. Based on the discussion in Section 3, this does not change $\mathbf{y}(0)$ since the joint would not change its position or direction for the last added b reversal points. Moreover, it should be noted that the reversal points are ordered from $t = 0$ to $t = T$ meaning that the algorithm starts at x_0 and then moves to x_{rev}^1 followed by x_{rev}^2 and so on and finally moves to x_T and the added reversal points would come after the last reversal points. Therefore, the idea of adding b reversal points does not change the initial state of sliders since moving from $x(T)$ to $x(T)$, i.e. $\Delta x_{rev} = x(T) - x(T) = 0$, would not affect the state of sliders. It should be mentioned that it seems plausible that the number of reversal points change from function evaluation to function evaluation. In this case, we use the same procedure that is used when the number of reversal points changes from iteration to iteration.

5. Results and discussion

A 3DOF system with three Iwan elements was chosen in order to evaluate the performance of the method. The system parameters can be found in Table 5, where F_s, K_t, χ and β are the Iwan parameters as described in [6]. Since this system involves three Iwan joints between each of the masses as depicted in Fig. 6, it is a challenging test case for the proposed method, HIRP. To calculate the periodic orbit for a range of different forcing frequencies, the procedure described in Section 4 was repeated for various force amplitudes. As the force amplitude increases, the number of slipped Coulomb sliders increases and consequently, the amount of dissipated energy also increases. Hence, at higher force amplitudes the system shows higher effective damping due to the Iwan joints. This is exhibited in Fig. 7 as a lowering and distortion of the peaks as the force amplitude increases, indicating increased nonlinearity in the system. The presence of Iwan joints also decreases the resonant frequency of the system somewhat. This softening nonlinear behavior is as expected because the system loses stiffness as more of the sliders transition from stuck (behaving as springs) to sliding, as was also seen in [45]. The results also show that the adaptive step size algorithm caused the continuation procedure to

Table 5
Linear and nonlinear parameters of the SDOF system studied. For this system, $\mathbf{F}_{ext} = \alpha \mathbf{F}_0$ where $\alpha = 3, 2, 1, 0.5, (1/3), 0.1$.

Parameter	Value
K_{lin} (N/m)	800
ζ_{lin}	1×10^{-2}
M (kg)	2
F_s (N)	100
K_T (N/m)	500
χ	−0.5
β	5
$\mathbf{F}_0$(N)	$[1, 2, -1]$

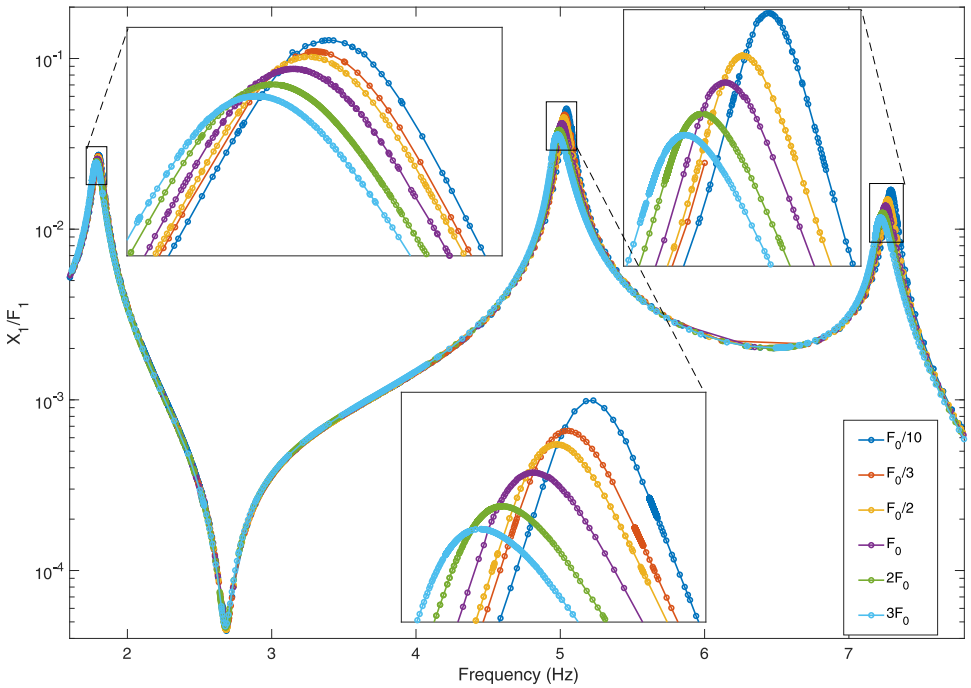

Fig. 7. The frequency response function of the 3DOF system shown in Fig. 6 for the different force amplitudes.

use a smaller step size near the resonances in order to follow the bends and corners in the resonant peak. This increases the density of the markers around the peak and also the computational cost around the peaks. For the same reason, more time is required to compute the FRF at a higher force amplitudes.

In order to better understand the computed steady-state response of the system, a few points are chosen from some of the FRF curves at $f = 4.98$ Hz and their steady-state response, nonlinear force and stiffness are plotted in Fig. 8. The first row shows the response of the first mass, $x_1(t)$, which is normalized by the maximum value of displacement $max(x_1(t))$. One can observe that, although there is no visible harmonic distortion, the higher load amplitude leads to significant phase lag in the response. The nonlinear force in the first Iwan joint, f_{nl} in Eq. (4), normalized by F_S from Table 5, is shown in the second row of Fig. 8. As with the response of the system, more phase lag can be observed in the nonlinear force as the force amplitude becomes larger, although for most cases shown the nonlinear force is a small fraction of F_S. The tangent stiffness shown in the third row decreases as the displacement increases, causing a larger number of sliders to slip. For the largest force amplitude considered of $F_{ext} = 3F_0$, it can be seen in the last row that all of the sliders except for the five strongest ones are slipping, which indicates that the joint is near macro-slip. For the other cases, the joint behaves as if in micro-slip during the whole period. The last row of Fig. 8 shows several instances where the number of slipped sliders decreases abruptly. This corresponds to the instants right after the joint has changed its direction, when many of the sliders become stuck again. It is also important to note that this last row shows that the slipping of the sliders is also periodic. Furthermore, it is interesting to investigate the time histories of some of the sliders near resonance. Fig. 9 shows the time response of the 50th, 140th, 142th, 144th and 150th sliders over one period for the solution at $f = 4.9813$ Hz for various excitation force levels $F_{ext} = 3F_0, 2F_0, F_0, 0.1F_0$. Since the 150th slider is not slipping for all the cases, the system is in a state of micro-slip. It can be seen that the response of many of sliders consists of the highly non-sinusoidal nature meaning that the derivative of their response is clearly discontinuous. This shows one the key advantages of the proposed method; all of the states of the sliders were captured implicitly; their responses were inferred from the physical states of the system and from the reversal

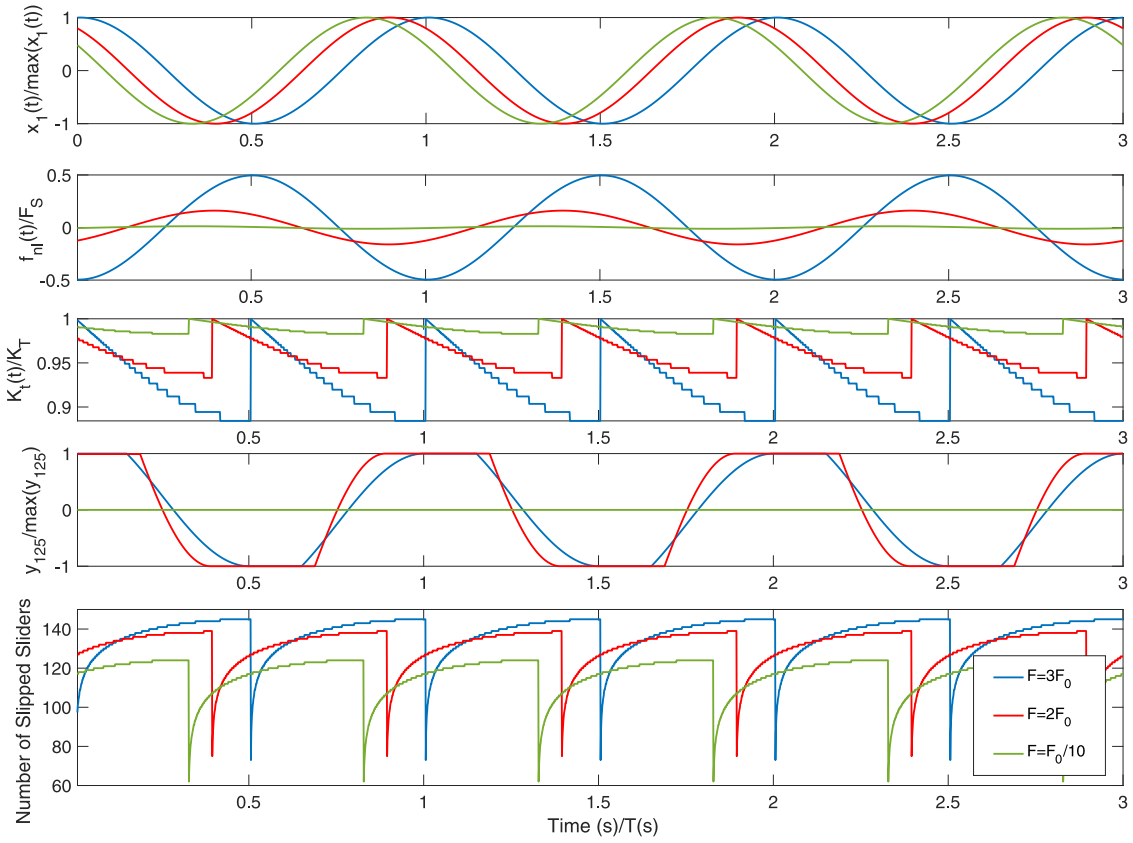

Fig. 8. Comparing the displacements, fraction of slipped sliders, nonlinear restoring fore and the position of the 75th slider for different force amplitudes.

points in the response. In contrast, if a conventional continuation method had been applied to this system, one needed to include all 150 displacements across each slider as states so that the slider state (stick/slip) could be tracked.

In order to verify that the FRFs computed were accurate, the response was computed for a point with $F = 2F_0$ and close to the resonant frequency. The response was initiated with zero initial conditions and integrated over 125 periods. The result of direct integration is compared to the steady-state response computed by the proposed algorithm (replicated 125 times) in Fig. 10. One can see that the two curves overlay towards the end of the time response, demonstrating that the FRFs found by the continuation algorithm are accurate. Furthermore, this figure illustrates the computational advantage that is achieved by using the proposed continuation routine rather than direct time integration. When direct integration is used, more than five minutes of computation time is required to obtain only one point on the FRF (it depends on the number of time samples and the forcing frequency). In contrast, the time required to find the steady-state response at this one point by the proposed algorithm was about ten seconds. It would clearly be highly more expensive to compute the complete frequency response functions shown in Fig. 7 using direct integration, but the calculation is easily within reach using the proposed algorithm.

As was noted previously, one important feature of the proposed algorithm was a strategy for adapting the finite difference step size at each frequency line. In the cases presented above, the algorithm typically converged after 2–3 iterations, so that this algorithm was not activated. However, there about 5 frequency lines near each resonance where between 6–12 iterations were required; at some of these frequencies the algorithm would have failed to converge if the finite difference step size was not adapted using the proposed algorithm.

6. S4 Beam

In order to verify the performance of the proposed methods on a realistic model, the S4 Beam that was studied in [8,33,46] was also investigated in this paper. Photos of the structure are shown in Fig. 11. The S4Beam consists of two beams bolted together, but to simplify the model, spiders were used to reduce the contact patch on each beam to a single virtual node (with 6 DOF), as is shown in Fig. 12. (The interfaces and slave nodes are actually coincident and they are shown expanded in Fig. 12 only for visualization purposes.) The spiders used RBAR elements (i.e. using NASTRAN's naming convention) to connect the contact surfaces in an average sense (i.e. rather than rigidly) to the slave node. Then, each beam was reduced using the Hurty/Craig–Bampton (HCB) [47] approach, retaining only the 6 DOF at each spider at each of the four interfaces (24 DOF total) as well as 30 fixed-interface modes, for a total

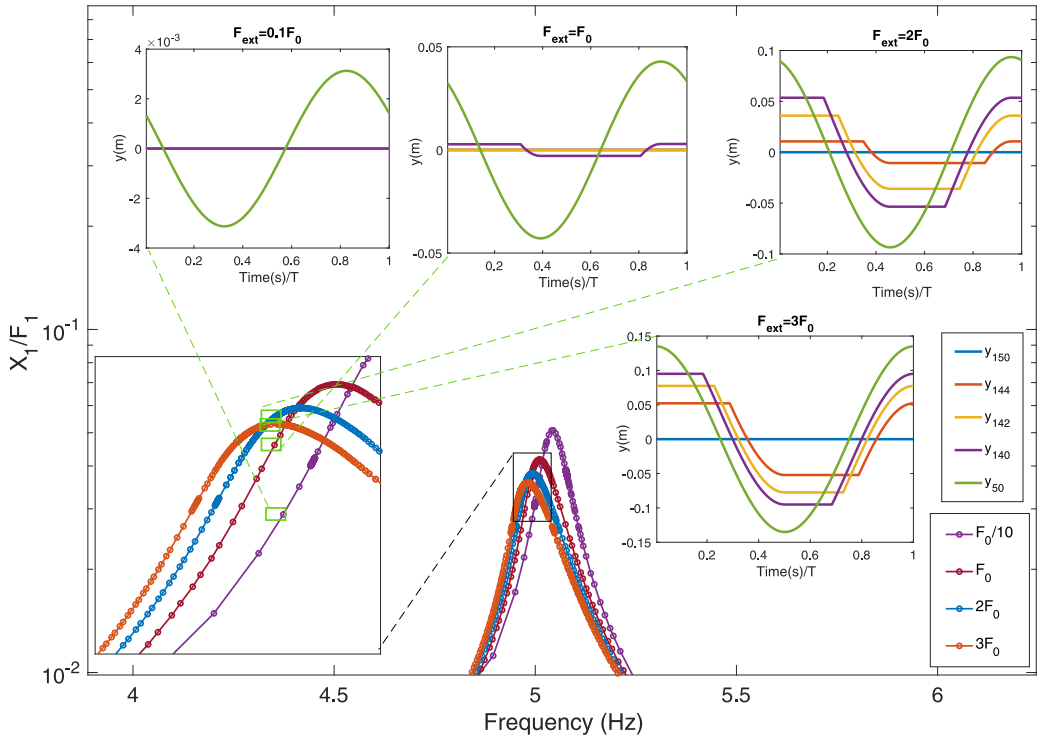

Fig. 9. The time response of the 50th, 140th, 142th, 144th and 150th slider over a period at $f = 4.9813$ Hz for different force levels.

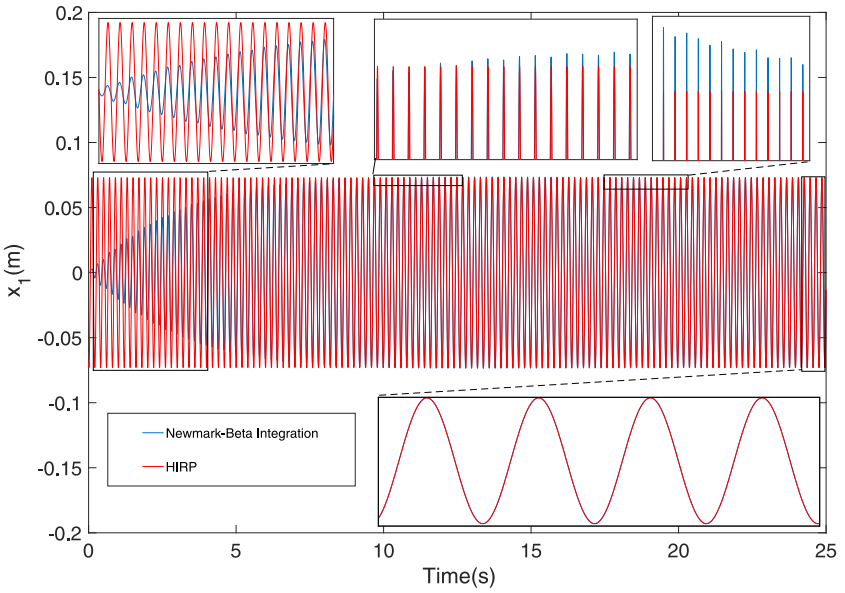

Fig. 10. Comparison between the results obtained from the proposed method and the results obtained from direct integration (Newmark-Beta) for $T = 0.2$ s for $F_{ext} = 2F_0$.

of 54 DOF. In order to connect the contact patches, six linear springs were inserted between the virtual nodes and updated to match the linear natural frequencies obtained from the test structures shown in Fig. 11. The spring constants used are given in Table 6. For an in-depth discussion of the modeling and model updating refer to [33,48]. In this paper, three of the linear springs were replaced with Iwan elements (x, z and R_y directions) (6 Iwan elements in total). The Iwan parameters are shown in Table 6 where F_s, K_t, χ and β are the Iwan parameters as described in [6]; 150 sliders were used for each Iwan element.

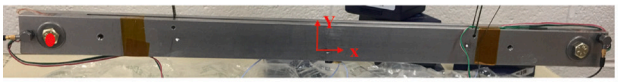

(a) The S4 Beam side view

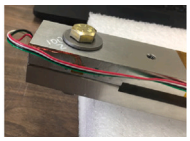

(b) The S4 Beam: The bolt and the contact surfaces

Fig. 11. Photos of the actual S4 beam. A harmonic force is applied at the node shown with a red circle in the z-direction.

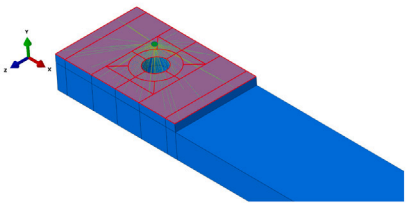

(a) S4 Beam: an RBAR element is used for each contact patch

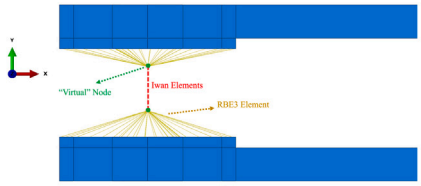

(b) S4 Beam: The Iwan joint is inserted between the virtual nodes

Fig. 12. (a) and (b): Coupling the contact patches to the virtual nodes by using RBAR elements. The virtual nodes were then connected by three Iwan joints in x, y and R_z directions.

Table 6
Linear and non-linear parameters of the S4 Beam.

Parameter	Value
$[K_{lin_x}, K_{lin_y}, K_{lin_z}]$	$[2.37\times10^7, 1.77\times10^8, 1.51\times10^8]$ (N/m)
$[K_{lin_{R_x}}, K_{lin_{R_y}}, K_{lin_{R_z}}]$	$[3.55\times10^8, 3.65\times10^5, 2.16\times10^6]$ (N − m/rad)
ζ_{lin}	4×10^{-4}
F_s	68.156 (N)
K_t	2.077×10^6 (N/m)
χ	−0.61533
β	0.062146

Because this system was considerably more expensive than the 3DOF system in the previous section, the frequency response was computed at only one frequency, i.e at $f_n = 331.78$ Hz or very near the second natural frequency, with a force applied at the red point shown in Fig. 11a. The second mode was found to be most strongly affected by the nonlinearity in the joint in [8]. The initial conditions computed by the proposed algorithm were used to integrate the model over nine periods in order to verify that they were periodic, revealing that the maximum error in periodicity at any of the slave nodes was less than one percent. The first row of Fig. 13 shows the response of the system at the joints in the x-direction for different force levels, the second row depicts the hysteresis curve for each Iwan element in the x-direction, the third row represents the number of slipped sliders at each joint and the fourth row shows the stiffness of each joint in x-direction over three periods. As expected, the higher force amplitudes lead to more nonlinear behavior in the system, as can be observed in the third row of Fig. 13. This results in more phase lag in the response as shown in the first row of Fig. 13, more dissipation of energy as observed in the second row and less stiffness of the joint depicted in the fourth row of Fig. 13. For this S4 Beam model (54 total DOF with 6 Iwan elements), the steady-state response of the system was computed in less than 15 min for each force level. In contrast, the system was integrated for over 5 h and the steady-state response had still not been obtained to similar accuracy.

7. Conclusion

This paper proposed a new time-domain continuation algorithm that can compute the steady-state response of hysteretic systems containing frictional devices modeled by the Coulomb sliders, e.g. Iwan joints. These systems are challenging to model because the state of sliders must be considered, and there are typically many sliders and their states have discontinuous derivatives. In order to address this, a quasi-static algorithm was introduced in this paper which uses the reversal points to evaluate the initial state of sliders. In this way, while the effect of the sliders are considered in the solution, only a few state variables need to be added to the problem (e.g. two states for weakly nonlinear cases). Due to quasi-static nature of the proposed algorithm, the added cost to the solution is small and the algorithm proved capable of computing the steady-state response very accurately. To accommodate with the added state variables (reversal points), the continuation method was modified. The finite difference method was used to find the Jacobians with respect to the reversal points and the other state variables. The efficiency and robustness of the solution was improved by adapting the step size used to compute the finite difference derivatives.

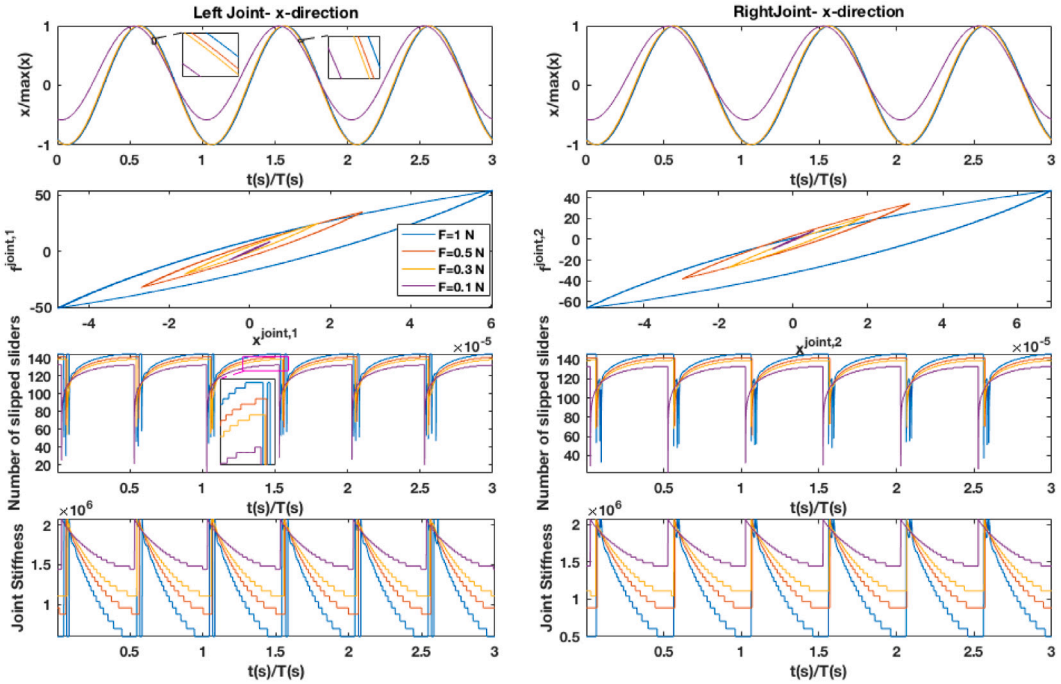

Fig. 13. The steady-state response obtained for the S4 beam excited at its second mode, $f_n = 331.78$ Hz, and comparing the displacements, number of slipped sliders, hysteresis curve and the stiffness of the joints for different force amplitudes.

As the first test case, the nonlinear FRFs of a MDOF system with multiple Iwan elements were computed. The algorithm was found to compute the periodic response with high accuracy as compared to direct time integration, but with a huge reduction in the computational cost. The frequency responses obtained were shown to provide several insights into the behavior of the Iwan joints in steady-state vibration; results with this level of resolution have not been presented in any prior publication of which the authors are aware. The algorithm was also applied to a more complicated model, a 54-DOF model of the S4 Beam, and found to provide plausible results at a few key frequencies. Direct integration was not feasible on that model. Indeed, many hours would have been required to find the FRFs of that system over a large number of frequencies. Hence, while the proposed algorithm does make FRF computation possible for realistic structures, it remains quite expensive.

Most of the computational cost of the proposed algorithm is in using the Newmark-Beta integration method repeatedly over one period. This contributes about 90% of the total run time. Indeed, less than 0.5 percent of the total time is spent in the algorithm that computes the initial state of sliders. At each forcing frequency, several iterations are typically needed to converge on the steady-state response of the system. Future works may seek to find faster time integration methods that are applicable to these classes of systems, so that larger systems could be tackled more comfortably.

CRediT authorship contribution statement

Seyed Iman Zare Estakhraji: Investigation, Conceptualization, Methodology, Data curation, Software, Writing – original draft, Writing – review & editing. **Matthew S. Allen:** Conceptualization, Methodology, Software, Writing – review & editing, Supervision.

Declaration of competing interest

The authors declare that they have no known competing financial interests or personal relationships that could have appeared to influence the work reported in this paper.

Acknowledgment

This material is based in part upon work supported by the National Science Foundation, United States of America under Grant Number CMMI-1561810. Any opinions, findings, and conclusions or recommendations expressed in this material are those of the author(s) and do not necessarily reflect the views of the National Science Foundation.

Appendix A. Supplementary data

Supplementary material related to this article can be found online at https://doi.org/10.1016/j.jsv.2021.116342.

References

[1] W.D. Iwan, The steady-state response of a two-degree-of-freedom bilinear hysteretic system, J. Appl. Mech. Trans. ASME 32 (1) (1964) 151–156, http://dx.doi.org/10.1115/1.3625711.
[2] R.M. Rosenberg, On nonlinear vibrations of systems with many degrees of freedom, in: Adv. Appl. Mech., 9, Elsevier, 1966, pp. 155–242.
[3] R.M. Rosenberg, Steady-state forced vibrations, Int. J. NonLinear Mech. 1 (2) (1966) 95–108, http://dx.doi.org/10.1016/0020-7462(66)90023-0.
[4] W.D. Iwan, A distributed element model for hysteresis and its steady-state dynamic response, J. Appl. Mech. (ISSN: 0021-8936) 33 (4) (1966) 893–900, http://dx.doi.org/10.1115/1.3625199.
[5] B.J. Deaner, M.S. Allen, M.J. Starr, D.J. Segalman, H. Sumali, Application of viscous and iwan modal damping models to experimental measurements from bolted structures, J. Vib. Acoust. Trans. ASME (ISSN: 15288927) 137 (2) (2015) 12, http://dx.doi.org/10.1115/1.4029074.
[6] D.J. Segalman, A four-parameter iwan model for lap-type joints, J. Appl. Mech. 72 (5) (2005) 752–760.
[7] I. Zare, M.S. Allen, Adapting a contact-mechanics algorithm to predict damping in bolted joints using quasi-static modal analysis, Int. J. Mech. Sci. 189 (2021) 105982, http://dx.doi.org/10.1016/j.ijmecsci.2020.105982.
[8] E. Jewell, M.S. Allen, I. Zare, M. Wall, Application of quasi-static modal analysis to a finite element model and experimental correlation, J. Sound Vib. 479 (2020) 115376.
[9] J.H. Griffin, A. Sinha, The interaction between mistiming and friction in the forced response of bladed disk assemblies, J. Eng. Gas Turbines Power 107 (1) (1985) 205–211.
[10] A. Sinha, J.H. Griffin, Effects of friction dampers on aerodynamically unstable rotor stages, AIAA J. 23 (2) (1985) 262–270.
[11] C.-H. Menq, J. Bielak, J.H. Griffin, The influence of microslip on vibratory response, part i: a new microslip model, J. Sound Vib. 107 (2) (1986) 279–293.
[12] M. Mitra, B.I. Epureanu, Dynamic modeling and projection-based reduction methods for bladed disks with nonlinear frictional and intermittent contact interfaces, Appl. Mech. Rev. 71 (5) (2019).
[13] R.A. Ibrahim, C.L. Pettit, Uncertainties and dynamic problems of bolted joints and other fasteners, J. Sound Vib. 279 (3–5) (2005) 857–936.
[14] D. Li, C. Xu, D. Botto, Z. Zhang, M. Gola, A fretting test apparatus for measuring friction hysteresis of bolted joints, Tribol. Int. (2020) 106431.
[15] M. Groper, Microslip and macroslip in bolted joints, Exp. Mech. 25 (2) (1985) 171–174.
[16] L. Gaul, R. Nitsche, The role of friction in mechanical joints, Appl. Mech. Rev. 54 (2) (2001) 93–106, http://dx.doi.org/10.1115/1.3097294.
[17] R. Wang, A.D. Crocombe, G. Richardson, C.I. Underwood, Energy dissipation in spacecraft structures incorporating bolted joints operating in macroslip, J. Aerosp. Eng. 21 (1) (2008) 19–26.
[18] C. Padmanabhan, R. Singh, Analysis of periodically excited non-linear systems by a parametric continuation technique, J. Sound Vib. 184 (1) (1995) 35–58.
[19] L. Charroyer, O. Chiello, et al., Estimation of self-sustained vibration for a finite element brake model based on the shooting method with a reduced basis approximation of initial conditions, J. Sound Vib. 468 (2020) 115050.
[20] E.J. Berger, Friction modeling for dynamic system simulation, Appl. Mech. Rev. 55 (6) (2002) 535–577.
[21] V. Van Geffen, A study of friction models and friction compensation, 2009.
[22] C.C. De Wit, H. Olsson, K.J. Astrom, P. Lischinsky, A new model for control of systems with friction, IEEE Trans. Automat. Control 40 (3) (1995) 419–425.
[23] L. Freidovich, A. Robertsson, A. Shiriaev, R. Johansson, Lugre-model-based friction compensation, IEEE Trans. Control Syst. Technol. 18 (1) (2009) 194–200.
[24] J. Swevers, F. Al-Bender, C.G. Ganseman, T. Projogo, An integrated friction model structure with improved presliding behavior for accurate friction compensation, IEEE Trans. Automat. Control 45 (4) (2000) 675–686.
[25] R. Bouc, Forced vibrations of mechanical systems with hysteresis, in: Proc. Fourth Conf. Nonlinear Oscil. Prague, 1967, 1967.
[26] M. Oldfield, H. Ouyang, J.E. Mottershead, Simplified models of bolted joints under harmonic loading, Comput. Struct. 84 (1–2) (2005) 25–33.
[27] W.D. Iwan, Steady-state dynamic response of a limited slip system, J. Appl. Mech. Trans. ASME 35 (2) (1964) 322–326, http://dx.doi.org/10.1115/1.3601198.
[28] W.D. Iwan, R.K. Miller, The steady-state response of systems with spatially localized non-linearity, Int. J. NonLinear Mech. 12 (3) (1977) 165–173.
[29] D.J. Segalman, D.L. Gregory, M.J. Starr, B.R. Resor, M.D. Jew, J.P. Lauffer, N.M. Ames, Handbook on Dynamics of Jointed Structures, Tech. Rep., Sandia National Laboratories, Albuquerque, NM 87185, 2009.
[30] D.J. Segalman, M.J. Starr, Iwan models and their provenance, in: Int. Des. Eng. Tech. Conf. Comput. Inf. Eng. Conf., Vol. 45004, American Society of Mechanical Engineers, 2012, pp. 441–449.
[31] M.S. Bonney, B.A. Robertson, M. Mignolet, F. Schempp, M.R. Brake, Experimental determination of frictional interface models, in: Dyn. Coupled Struct. Vol. 4, Springer, 2016, pp. 473–490.
[32] R.M. Lacayo, B.J. Deaner, M.S. Allen, A numerical study on the limitations of modal iwan models for impulsive excitations, J. Sound Vib. (ISSN: 0022460X) 390 (2017) 118–140.
[33] A. Singh, M. Wall, M.S. Allen, R.J. Kuether, Spider configurations for models with discrete iwan elements, in: Nonlinear Struct. Syst. Vol. 1, Springer, 2020, pp. 25–38.
[34] P.-T. Spanos, Hysteretic structural vibrations under random load, J. Acoust. Soc. Am. 65 (2) (1979) 404–410.
[35] M.A. Dokainish, K. Subbaraj, A survey of direct time-integration methods in computational structural dynamics—I. Explicit methods, Comput. Struct. 32 (6) (1989) 1371–1386.
[36] K. Subbaraj, M.A. Dokainish, A survey of direct time-integration methods in computational structural dynamics—II. Implicit methods, Comput. Struct. 32 (6) (1989) 1387–1401.
[37] L. Fu-hua, A numerical treatment of the periodic solutions of non-linear vibration systems, Appl. Math. Mech. 4 (4) (1983) 525–546.
[38] P. Sundararajan, S.T. Noah, Dynamics of forced nonlinear systems using shooting/are-length continuation method-application to rotor systems, J. Vib. Acoust. Trans. ASME 119 (1) (1997) 9–20, http://dx.doi.org/10.1115/1.2889694.
[39] E.L. Allgower, K. Georg, Introduction to Numerical Continuation Methods, SIAM, 2003.
[40] P. Malatkar, A.H. Nayfeh, Steady-state dynamics of a linear structure weakly coupled to an essentially nonlinear oscillator, Nonlinear Dynam. 47 (1–3) (2007) 167–179.
[41] A.H. Nayfeh, B. Balachandran, Applied Nonlinear Dynamics: Analytical, Computational, and Experimental Methods, John Wiley & Sons, 2008.
[42] M. Peeters, R. Virguie, G. Serandour, G. Kerschen, J.C. Golinval, Nonlinear normal modes, part II: Toward a practical computation using numerical continuation techniques, Mech. Syst. Signal Process. 23 (1) (2009) 195–216.
[43] M.W. Sracic, M.S. Allen, Numerical continuation of periodic orbits for harmonically forced nonlinear systems, in: T. Proulx (Ed.), Civil Engineering Topics, Vol. 4, Springer New York, New York, NY, 2011, pp. 51–69.
[44] R.D. Cook, D.S. Malkus, M.E. Plesha, R.J. Witt, Concepts and Applications of Finite Element Analysis, Vol. 4, Wiley New York, 1974.
[45] M. Ghienne, L. Laurent, C. Blanzé, Robust characterization of the vibrational behaviour of light assembled structures with random parameters, Mech. Syst. Signal Process. 136 (2020) 106510.
[46] M. Wall, M.S. Allen, I. Zare, Predicting S4 beam joint nonlinearity using quasi-static modal analysis, in: Nonlinear Struct. Syst. Vol. 1, Springer, 2020, pp. 39–51.
[47] R.R. Craig, M.C.C. Bampton, Coupling of substructures for dynamic analyses, AIAA J. 6 (7) (1968) 1313–1319, http://dx.doi.org/10.2514/3.4741.
[48] A. Singh, M.S. Allen, R.J. Kuether, Spider configurations for models with discrete iwan elements, Springer, 2021, submitted for publication,